Numerical investigation of a small footprint plasmonic Bragg grating structure with a high extinction ratio

Muhammad Ali Butt[1,2]

[1]*Department of Technical Cybernetics, Samara National Research University, 34 Moskovkoye Shosse, Samara 443086, Russia*
[2]*Institute of Microelectronics and Optoelectronics, Warsaw University of Technology, Koszykowa 75, 00-662 Warszawa, Poland*

Received August 19, 2020; accepted September 21, 2020; published September 30, 2020

Abstract—In this paper, miniaturized design of a plasmonic Bragg grating filter is investigated via the finite element method (FEM). The filter is based on a plasmonic metal-insulator-metal waveguide deposited on a quartz substrate. The corrugated Bragg grating designed for near-infrared wavelength range is structured on both sides of the waveguide. The spectral characteristics of the filter are studied by varying the geometric parameters of the filter design. As a result, the maximum *ER* and bandwidth of 36.2 dB and 173 nm are obtained at λ_{Bragg}=976 nm with a filter footprint as small as 1.0 × 8.75 μm^2, respectively. The *ER* and bandwidth can be further improved by increasing the number of grating periods and the strength of the grating, respectively. Moreover, the Bragg grating structure is quite receptive to the refractive index of the medium. These features allow the employment of materials such as polymers in the metal-insulator-metal waveguide which can be externally tuned or it can be used for refractive index sensing applications. The sensitivity of the proposed Bragg grating structure can offer a sensitivity of 950 nm/RIU. We believe that the study presented in this paper provides a guideline for the realization of small footprint plasmonic Bragg grating structures which can be employed in filter and refractive index sensing applications.

Bragg gratings have been broadly used in photonic circuits incorporated on a silicon-on-insulator (SOI) platform to realize functionalities such as filter, coupler, medical diagnostics, spectroscopy, display colour generation and sensing, among others [1-3]. Bragg gratings based on SOI platform can provide these filtering characteristics on a low-cost platform but the main downside is the requirement of long grating structures to obtain high extinction ratio (*ER*) [4-6]. It can be a major concern when filters with small footprints are preferred.

Surface plasmon polaritons (SPPs) are electromagnetic waves that propagate along the metal-insulator interface having an exponentially decaying field [7]. They offer the potential to develop highly integrated optical circuits due to their capability to overcome the diffraction limit of light. There are two main types of SPP based waveguide structures, namely: insulator-metal-insulator (IMI) and metal-insulator-metal (MIM) waveguides [7]. An MIM waveguide has the potential to squeeze the mode size down to a few tens of nanometer, which makes them an ideal candidate for nanoscale photonic devices. On the other hand, an IMI waveguide fails to do so. There are numerous plasmonic filter configurations that have been proposed such as ring resonator, Fabry-Perot resonator and Bragg grating, among others [8-10]. The Bragg grating based on the MIM structure can be realized by waveguide width modulation, waveguide core refractive index modulation and a combination of them [11]. Another significant application for the plasmonic Bragg grating is sensing, as the Bragg wavelength (λ_{Bragg}) is highly receptive to external environments such as temperature, pressure and refractive index [12-13].

In this letter, we numerically investigate the effect of geometric parameters on the performance of the plasmonic Bragg grating structure. Here, we have concentrated on obtaining a high extinction ratio (*ER*) of the Bragg grating filter, which is calculated as:

$$ER = 10 \times \log \frac{P_{out}}{P_{in}},$$

where P_{out} and P_{in} are the output and input power, respectively. The proposed plasmonic Bragg grating filter design is shown in Fig. 1. The metal and insulator materials are defined as gold (*Au*) and air, respectively. A metal-insulator-metal (MIM) waveguide with periodic corrugation is formed on both sides of the *Au* layer resulting in a Bragg grating pattern. The frequency-dependent complex relative permittivity of *Au* is characterized by the Lorentz-Drude model. The width of the MIM waveguide is represented as *w* which is fixed at 100 nm. *L* is the length of the segment where the waveguide width is *w* whereas *s* is the corrugated part while *d* is the strength of corrugation. Therefore the period (∧) can be written as ∧=*L*+*s*. To simplify the study *s* is fixed at 100 nm. The number of grating period is expressed as *N*. The TM mode of the MIM waveguide is excited by a plane wave and the transmission spectrum is obtained by line integration of the output port. As $w << \lambda_{incident}$, thus, only the fundamental TM mode can exist. The transmission spectrum and E-field distributions are simulated using the 2D-finite element method (FEM) with a scattering boundary condition. The EM-wave frequency domain (*emw*) is selected as a physics interface and modal analysis is added to the study. In COMSOL simulations, the subdomains of the device design are divided into triangular mesh elements with an *extra-fine* mesh grid

size for the MIN waveguide and a *finer* mesh grid for the air domain. This produces precise simulation results within the available computational resources. It is necessary to model a domain with open boundaries, that is such boundaries of the computational domain through which an EM wave can travel without reflection. An open geometry is estimated by employing scattering boundary conditions (SBC) at the outer edges of the *FEM* simulation window.

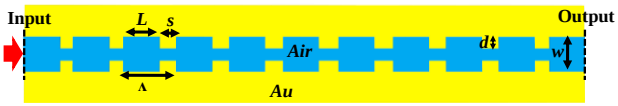

Fig. 1. 2D representation of a plasmonic Bragg grating filter.

Here, the spectral characteristics of the Bragg grating are studied by individually varying the geometric parameters of the structure. At first, the effect on λ_{Bragg} and *ER* is examined by varying Λ of the Bragg grating. To simplify the mechanism, *s* is fixed at 100 nm whereas *L* is varied between 200 nm and 300 nm with a step size of 25 nm. The remaining parameters such as *d*, *w* and *N* are set at 20 nm, 100 nm and 15, respectively. From Fig. 2a, it can be observed that with increasing *L* (or Λ), λ_{Bragg} performs a redshift with a decrease in *ER*. At *L*=200 nm, λ_{Bragg}=850 nm having *ER*= 24.8 dB is obtained which shifts to λ_{Bragg}=1114 nm with a slight decrease in *ER*=19.73 dB at *L*= 300 nm as shown in Fig. 2a. To improve the *ER*, we can either increase *d* or *N*. However, in the former case, the bandwidth can also increase. In the second stage, we analyzed the effect of *d* on the *ER* of the filter. The remaining parameters such as *L*, *s*, *w* and *N* are fixed at 250 nm, 100 nm, 100 nm and 15, respectively. From Fig. 2b, it can be seen that there is a noteworthy rise in the *ER* of the filter along with the bandwidth as *d* increases. The spectral characteristics of the filter are shown in Table 1.

Table 1. Spectral characteristics of the Bragg grating filter for different values of *d*.

d (nm)	λ_{Bragg} *(nm)*	*ER (dB)*	*Bandwidth (nm)*
10	918	10.34	86
15	946	15.8	116
20	982	21.9	157
25	1030	28.74	218.8
30	1094	36.47	327

The number of periods (*N*) has a vital impact on the *ER* of the filter. We simulated plasmonic Bragg filter of Λ=350 nm and different values of *N*. The *ER* is plotted for *N*= 5, 10, 15, 20 and 25 as shown in Fig. 2 c. We can find an enhancement in *ER* as *N* increases with a slight change in the bandwidth of the filter. The λ_{Bragg}, *ER*, bandwidth and the footprint of the filter are presented in Table 2. This footprint is smaller than most of the previously reported filters [14-16].

Table 2: Spectral characteristics of the Bragg grating filter for different values of *N*.

N	λ_{Bragg} *(nm)*	*ER (dB)*	*Bandwidth (nm)*	*Footprint (μm^2)*
5	1016	7.9	245	1×1.75
10	988	14.8	194	1×3.5
15	982	21.9	188	1×5.25
20	978	29	179	1×7
25	976	36.2	173	1×8.75

It is worth noting that the *ER* of the proposed Bragg grating filter can be further increased by increasing the value of *N*. To verify the idea, we have shown only limited values in this paper.

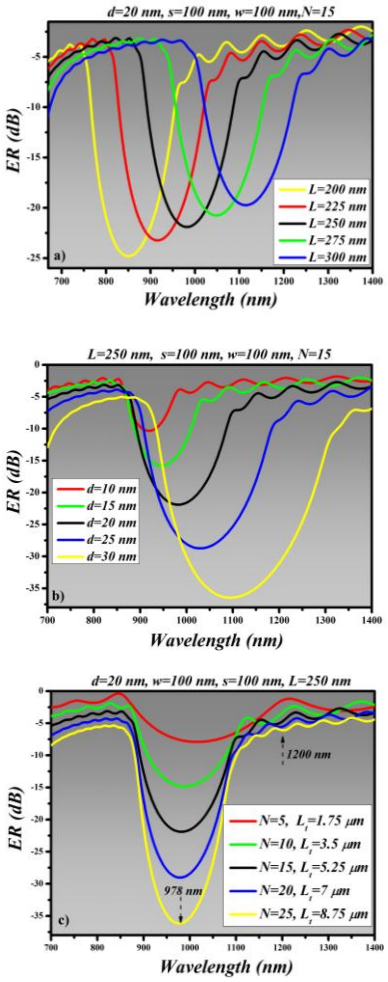

Fig.2. Extinction ratio dependent on, a) *L*, b) *d* and, c) *N*. The remaining parameters of the grating structure is mentioned in the paper.

The E-field distribution of the propagating mode at λ= 978 nm and λ=1200 nm is plotted for *N*=25 as shown in Fig. 3. The remaining geometric parameters of the filter are the same as those used in Fig. 2c. At *λ*=978 nm, the Bragg condition is satisfied, which results in a strong reflection of light (ER=36.2 dB) whereas *λ*=1200 nm doesn't obey the Bragg grating condition, and as a result, it propagates throughout the grating as shown in Figure 3b.

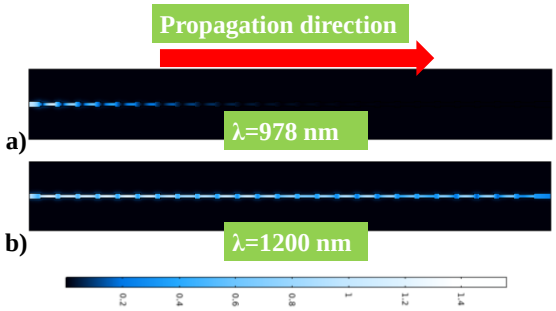

Fig. 3. E-field distribution in the Bragg grating structure at, a) λ=978 nm, b) λ=1200 nm.

Moreover, λ_{Bragg} can be tuned by varying the refractive index of the ambient medium, which results in variation of the effective refractive index of the propagating mode. For this analysis, the Bragg grating structure with parameters such as *L*, *s*, *w*, *d* and *N* fixed at 250 nm, 100 nm, 100 nm, 20 nm and 25, respectively is used. From Fig. 4 it can be seen that λ_{Bragg}=977 nm at n=1.0 experiences a redshift to 1262 nm at n=1.3 without changing the *ER* of the filter. Additionally, the proposed Bragg grating structure can be used in refractive index sensing applications where the sensitivity (*S*) can be calculated as [17-18]:

$$S=\Delta\lambda_{Bragg}/\Delta n,$$

where $\Delta\lambda_{Bragg}$ and Δn are the change in Bragg wavelength and refractive index, respectively. The proposed structure offers an *S*=950 nm/RIU, which is higher than several previously proposed plasmonic sensors [19-20].

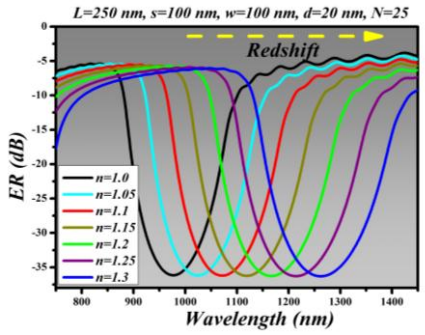

Fig. 4. The transmission spectrum of the Bragg grating structure versus the ambient refractive index.

In conclusion, we can say that a miniaturized design of a plasmonic Bragg grating structure is proposed which can be utilized in both filter and refractive index sensing applications. The spectral characteristics of the grating structure are numerically investigated by varying the period, strength of the grating and number of periods. Based on our results, for *N*=25, the maximum *ER* and bandwidth of 36.2 dB and 173 nm are obtained with a filter footprint as small as 1 × 8.75 μm^2, respectively. We believe that the *ER* can be further increased by increasing the number of periods up to a limit where the plasmonic waveguide doesn't suffer from high propagation loss. Additionally, the Bragg grating structure is quite receptive to the refractive index of the medium. These characteristics allow the utilization of materials such as polymers in the metal-insulator-metal waveguide, which can be externally tuned or used for refractive index sensing applications. The sensitivity of the proposed Bragg grating structure can offer a sensitivity of 950 nm/RIU.

The author thanks the Samara National Research University and the Warsaw University of Technology for their support in completing this work.

References

[1] J. W. Field *et al*., 2019 Conference on Lasers and Electro-Optics Europe and European Quantum Electronics Conference (CLEO/Europe-EQEC), Munich, Germany (2019), doi: 10.1109/CLEOE-EQEC.2019.8871943.
[2] L. Cheng, S. Mao, Z. Li, Y. Han, H.Y. Fu, Micromachines **11**, 666 (2020).
[3] J. Missinne, N.T. Beneitez, M-A. Mattelin, A. Lamberti, G. Luyckx, W.V. Paepegem, G.V. Steenberge, Sensors **18**, 2717 (2018).
[4] M.A. Butt, S.N. Khonina, N.L. Kazanskiy, J. Modern Opt. **66**, 1172 (2019).
[5] H. Qiu, J. Jiang, P. Yu, T. Dai, J. Yang, H. Yu, X. Jiang, Opt. Lett. **41**, 2450 (2016).
[6] M.A. Butt, S.N. Khonina, N.L. Kazanskiy, Comp. Opt. **43**, 1079 (2019).
[7] N.L. Kazanskiy, S.N. Khonina, M.A. Butt, Physica E **117**, 113798 (2020).
[8] L. Lu *et al*., IEEE Photon. Technol. Lett. **22**, 1765 (2012).
[9] R. Negahdari, E. Rafiee, F. Emami, J. Electromagn. Waves Appl. **32**, 1925 (2018).
[10] M. Janfaza, M.A. Mansouri-Birjandi, Appl. Phys. B, **123**, 262 (2017).
[11] C. Wu, G. Song, L. Yu, J.H. Xiao, J. Modern Opt. **60**, 1217 (2013).
[12] J. Zhu, G. Wang, Results in Phys. **15**, 102763 (2019).
[13] Y. Binfeng, H. Guohua, C. Yiping, Opt. Expr. **22**, 28662 (2014).
[14] A.D. Simard, Y. Painchaud, S. Larochelle, Internat. Quantum Electr. Conference Lasers and Electro-Optics Europe, IEEE, Munich, Germany (2013).
[15] C. Klitis, G. Cantarella, M.J. Strain, M. Sorel, Opt. Lett. **42**, 3040 (2017).
[16] J. Ctyroky *et al*., Opt. Expr. **26**, 179 (2018).
[17] M.A. Butt, N.L. Kazanskiy, S.N. Khonina, Laser Phys. **30**, 016202 (2020).
[18] M.A. Butt, N.L. Kazanskiy, S.N. Khonina, J. Modern Opt. **66**, 1920 (2019).
[19] N.L. Kazanskiy, M.A. Butt, Photon. Lett. Poland **12**, 1 (2020).
[20] Z. Guo, K. Wen, Q. Hu, W. Lai, J. Lin, Y. Fang, Sensors **18**, 1348 (2018).

